Supporting Information

Red-shift emission and rapid up-conversion of B,N-containing electroluminescent materials via tuning intramolecular charge transfer

Yi-Hui He[a], Feng-Ming Xie[a,*], Hao-Ze Li[b], Kai-Zhang[c], Yang Shen[a], Feng Ding[a], Cheng-Yuan Wang[a], Yan-Qing Li[b,*], Jian-Xin Tang[a,c,*]

[a] *Jiangsu Key Laboratory for Carbon-Based Functional Materials & Devices, Institute of Functional Nano & Soft Materials (FUNSOM), Soochow University, Suzhou, Jiangsu 215123, China*

[b] *School of Physics and Electronic Science, East China Normal University, Shanghai 200062, China*

[c] *Macao Institute of Materials Science and Engineering (MIMSE), Faculty of Innovation Engineering, Macau University of Science and Technology, Taipa, Macao 999078, China*

* Corresponding authors.

E-mail addresses: fmxie@suda.edu.cn (F.-M. Xie), yqli@phy.ecnu.edu.cn (Y.-Q. Li), jxtang@suda.edu.cn (J.-X. Tang).

Keywords:

thermally activated delayed fluorescence; intramolecular charge transfer; fast up-conversion rate; orange-red electroluminescence; efficiency roll-off

Table of Contents

1. Experimental section

1.1 General Information. All commercially available reagents were used as received unless otherwise stated. ^{1}H NMR spectra were measured on a Bruker AVANCE III type NMR Spectrometer with the internal standard of tetramethylsilane (TMS). MALDI TOF-MS mass spectra were obtained from an Agilent 1260-6125 instrument. Thermal gravimetric analysis (TGA) was carried out with an HCT-2 instrument at a heating rate of 10 °C min^{-1} under nitrogen atmosphere. Organic films for optical measurements were fabricated by thermal evaporation under high vacuum onto clean quartz substrates. Ultraviolet–visible (UV-Vis) absorption and photoluminescence (PL) spectra were recorded on a Perkin-Elmer Lambda 750 UV-Vis spectrophotometer and a FM-4 type fluorescence spectrophotometer (JY company, French), respectively. Low-temperature phosphorescence spectra of the neat films were measured with a FLS 920 spectrometer (Einburgh Corporation) at 77 K. The absolute photoluminescence quantum yields (PLQYs) of the doped films were obtained with a C9920-02G type fluorescence spectrophotometer (HAMAMASTU, Japan) with an integrating sphere at room temperature under nitrogen atmosphere. Transient PL decay spectra were measured with a Quantaurus-Tau fluorescence lifetime spectrometer (C11367-03, Hamamatsu Photonics)

1.2 Electrochemical measurements. The electrochemical properties of BN-AC, BN-PXZ and BN-PZ were studied by cyclic voltammetry. As shown in **Figure S10**, the reduction potentials calculated from the onset of the oxidation curves are -0.95 eV, -0.74 eV and -0.19 eV for BN-AC, BN-PXZ and BN-PZ, respectively, vs. an Ag/Ag$^+$ standard, corresponding to the highest occupied molecular orbital (HOMO) levels of -5.33 eV, -5.14 eV and -4.58 eV, using ferrocene as a reference. The lowest unoccupied molecular orbital (LUMO) levels can be calculated by the HOMO value and the E$_g$s obtained from the absorption spectra, to be -2.74 eV, -2.55 eV and -1.99 eV, respectively.

1.3 Single-Crystal Structure. Single crystal measurement was carried out at room temperature on a Rigaku RAXIS RAPID diffractometer equipped with a graphite monochromated Mo-Ka radiation source. The crystal structure was determined via SHELXL-97 software program.

1.4 Theoretical calculations. The ground state geometries were optimized using density functional theory (DFT) with B3LYP/6-31G(d) basis set. Energies and transition properties were optimized for S_1, T_1 and T_2 using time-dependent density functional theory (TD-DFT) with B3LYP/6-31G(d) method. All calculation including torsion angles were performed using Gaussian 16 program.

1.5 Optical characterization of organic thin films. Organic films for optical measurements were fabricated by thermal evaporation under high vacuum onto clean quartz substrates. UV-vis absorption spectra were recorded by a Perkin-Elmer Lambda 750 UV-Vis spectrophotometer. Steady State fluorescence spectra, fluorescence lifetime, and quantum efficiency were carried out with a FM-4 type fluorescence spectrophotometer (JY company, French), Quantaurus-Tau fluorescence lifetime spectrometer (C11367-03, Hamamatsu Photonics) and C9920-02G type fluorescence spectrophotometer (HAMAMASTU, Japan), respectively.

1.6 Calculation Formulas for the Photophysical Parameters. The calculation of the kinetic parameters assumes that internal conversion process of the singlet exciton is the main nonradiative decay [S1, S2].

$$K_F = \Phi_F / \tau_F \qquad (1)$$

$$\Phi_{PL} = k_F / (k_F + k_{IC}) \qquad (2)$$

$$\Phi_p = k_F / (k_F + k_{IC} + k_{ISC}) \qquad (3)$$

$$\Phi_{ISC} = k_{ISC} / (k_F + k_{IC} + k_{ISC}) \qquad (4)$$

$$K_{TADF} = \Phi_{TADF} / (\Phi_{ISC} \times \tau_{TADF}) \qquad (5)$$

$$k_{RISC} = k_F \times k_{TADF} \times \Phi_{TADF} / (k_{ISC} \times \Phi_F) \qquad (6)$$

Where $\varPhi_{PL}$ is the total fluorescence quantum yield, $\varPhi_F$ is the prompt fluorescent component of $\varPhi_{PL}$, $\varPhi_{TADF}$ is the delayed fluorescent component of $\varPhi_{PL}$. τ_F is the lifetime of prompt fluorescent, τ_{TADF} is the lifetime of TADF, k_F is the rate constant of fluorescent. k_{IC} is the rate constant of internal conversion; k_{TADF}, k_{ISC}, k_{RISC} are the rate constants of TADF, intersystem crossing and reverse intersystem crossing, respectively. $\varPhi_{ISC}$ is the quantum efficiencies of ISC process, respectively.

1.7 Device Fabrication and Characterization. Devices were fabricated under vacuum level lower than 1×10^{-4} Pa for both organic and metal layers. ITO coated glasses with a sheet resistance of 15 Ω square^{-1} were used as the substrate and cleaned by ultra-purified water and organic solvents. Then the ITO glasses were irradiated in UV-ozone for 15 min. Organic materials were evaporated to ITO with rate of about 0.1 nm s^{-1}, while the LiF and Al were evaporated at rates of around 0.01 and 0.5 nm s^{-1}, respectively. The thickness of each layer during the evaporation was determined with the help of quartz crystal monitors. All the device fabrication and characterization steps were carried out at room temperature under ambient laboratory conditions. Current density-voltage-luminance (J-V-L) characteristics and EL spectra of the devices were measured simultaneously with a source meter (Keithley model 2400) and a luminance meter/spectrometer (Photo Research PR670). The CIE 1931 color coordinates were obtained from the EL spectra. The EQE values were calculated by assuming an ideal Lambertian emission profile. All device performances are test and verified at least three times and are repeatable under the circumstances illustrated above.

1.8 Synthesis of Materials
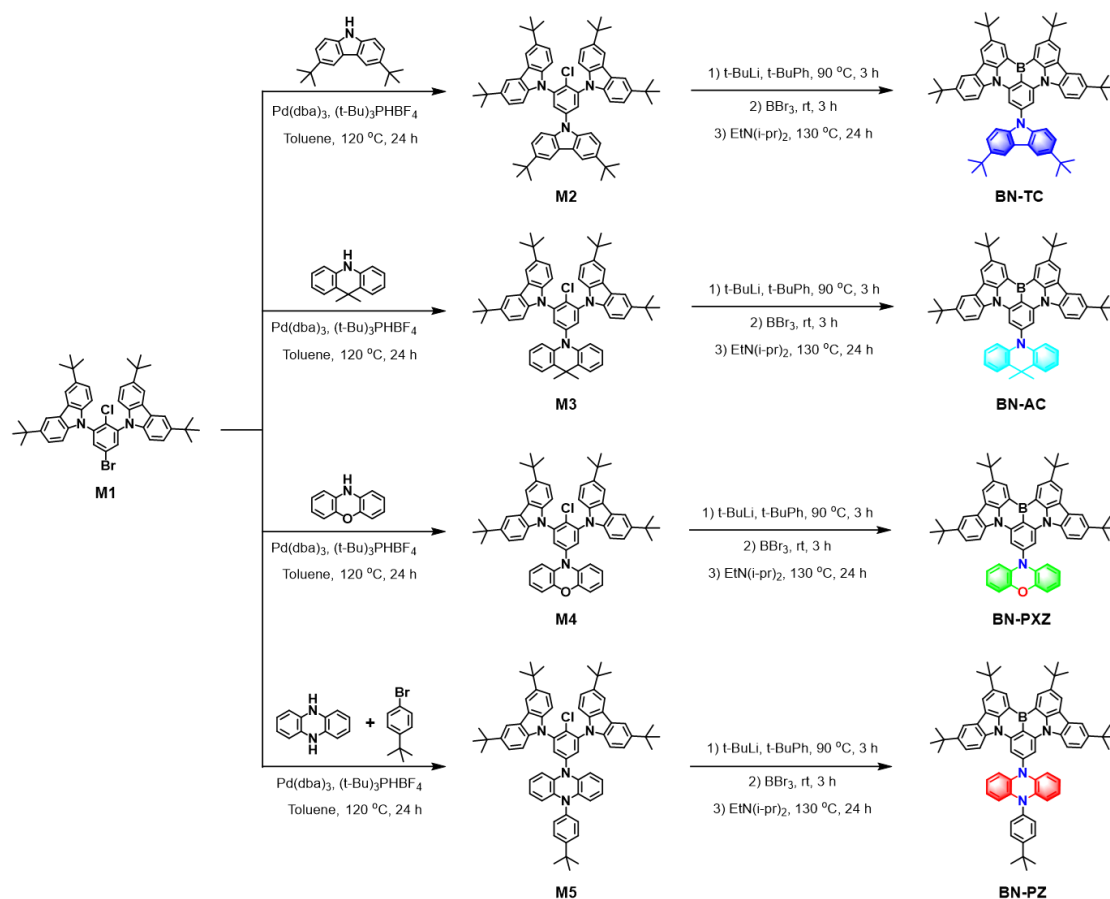
Scheme S1. Synthetic routes to BN-TC, BN-AC, BN-PXZ and BN-PZ.

Synthesis of 9,9'-(5-bromo-2-chloro-1,3-phenylene)bis(3,6-di-tert-butyl-9H-carbazole) (M1): The synthesis process was referred to the reported literature [S3].

Synthesis of 10-(4-chloro-3,5-bis(3,6-di-tert-butyl-9H-carbazol-9-yl)phenyl)-9,9-dimethyl-9,10-dihydroacridine (M2): The synthesis process was referred to the reported literature [S4].

Synthesis of BN-TC: The synthesis process was referred to the reported literature [S4].

Synthesis of 10-(4-chloro-3,5-bis(3,6-di-tert-butyl-9H-carbazol-9-yl)phenyl)-9,9-dimethyl-9,10-dihydroacridine (M3): M1 (1.00 g, 1.34 mmol), 9,9-dimethyl-9,10-dihydroacridine (0.34 g, 1.61 mmol) and 30 mL toluene were added to a 150 ml 3-

6

necked round bottom flask under nitrogen atmosphere. Then, (t-Bu)₃PHBF₄ (0.0040 g, 0.13 mmol) was slowly added and the reaction solution was stirred for 24 h at 120 °C. The reaction mixture was cooled to room temperature, and added to a saturated aqueous solution of sodium chloride (200 mL). Then the resulting mixture was extracted by dichloromethane for three times. The organic layer was concentrated and purified by flash chromatography through silica (chloroform/hexane: 1/5) to afford a white solid. Yield: 80.96% (1.08 g).

Synthesis of 10-(4-chloro-3,5-bis(3,6-di-tert-butyl-9H-carbazol-9-yl)phenyl)-10H-phenoxazine (M4): M4 was synthesized according to the same procedure as for **M3** by using 10H-phenoxazine (0.29 g, 1.61 mmol) instead 9,9-dimethyl-9,10-dihydroacridine. White solid (1.15 g, yield: 88.98%).

Synthesis of 5-(4-(tert-butyl)phenyl)-10-(4-chloro-3,5-bis(3,6-di-tert-butyl-9H-carbazol-9-yl)phenyl)-5,10-dihydrophenazine (M5): M5 was synthesized according to the same procedure as for **M3** by using 5,10-dihydrophenazine (0.29 g, 1.61 mmol) and 1-bromo-4-(tert-butyl)benzene (0.43 g, 2.00 mmol) instead 9,9-dimethyl-9,10-dihydroacridine. Yellow solid (0.87 g, yield: 50.58%).

Synthesis of BN-AC: M3 (1.00 g, 1.14 mmol) was fully dissolved in tert-butylbenzene (30 mL) in a round-bottom flask under nitrogen atmosphere. The reaction solution was cooled to 0 °C before tert-butyllithium (2.5 mL, 3.26 mmol, 1.3M in dichloromethane) was added and the solution was stirred for 2 h at 90 °C. After addition of boron tribromide (2.5 mL, 3.26 mmol, 1.3 M in dichloromethane) at 0 °C, the reaction mixture was stirred at room temperature for 2 hours. Then, N,N-diisopropylethylamine (1.5 mL, 9.12 mmol, ρ = 0.782 g/mL) was slowly added and the reaction solution was heated to 130 °C for 24 hours. After cooling to room-temperature, an aqueous solution of sodium acetate was added to the reaction mixture. Then the resulting mixture was extracted by dichloromethane for three times. The organic layer was concentrated and purified by flash chromatography through silica

(chloroform/hexane: 1/6) to afford a yellow solid. (0.43 g, yield: 44.48%). ^{1}H NMR (400 MHz, CDCl$_3$) δ 9.17 (d, J = 1.8 Hz, 2H), 8.49 (d, J = 1.8 Hz, 2H), 8.31 – 8.21 (m, 4H), 8.16 (d, J = 8.9 Hz, 2H), 7.61 – 7.48 (m, 4H), 7.03 – 6.95 (m, 4H), 6.68 – 6.59 (m, 2H), 1.84 (s, 6H), 1.69 (s, 18H), 1.47 (s, 18H). ^{13}C NMR (101 MHz, CDCl$_3$) δ 146.3, 145.7, 145.1, 141.6, 140.7, 138.1, 130.4, 129.9, 127.1, 126.7, 125.4, 124.6, 123.8, 120.9, 117.3, 114.6, 114.2, 109.8, 35.2, 34.8, 32.2, 31.7, 31.6. MALDI-TOF-MS (m/z) of C$_{61}$H$_{62}$BN$_3$ for [M]$^+$, calcd: 847.50; found: 847.309.

Synthesis of BN-PXZ: BN-PXZ was synthesized according to the same procedure as for BN-AC by using **M4** (1.00 g, 1.18 mmol) instead **M3**. BN-PXZ (0.57 g, yield: 58.77%) was obtained as yellow solid. ^{1}H NMR (400 MHz, CDCl$_3$) δ 9.16 (d, J = 1.7 Hz, 2H), 8.49 (d, J = 1.7 Hz, 2H), 8.26 (dd, J = 11.2, 9.6 Hz, 6H), 7.61 (dd, J = 8.8, 2.0 Hz, 2H), 6.81 (d, J = 7.8 Hz, 2H), 6.65 (dd, J = 24.7, 16.7 Hz, 4H), 6.28 (d, J = 7.8 Hz, 2H), 1.69 (s, 18H), 1.49 (s, 18H). ^{13}C NMR (101 MHz, CDCl$_3$) δ 146.4, 145.9, 145.2, 141.6, 138.1, 129.9, 127.1, 124.7, 123.9, 123.6, 121.0, 117.3, 114.2, 113.6, 35.2, 34.8, 32.2, 31.8. MALDI-TOF-MS (m/z) of C$_{58}$H$_{56}$BN$_3$O for [M]$^+$, calcd: 821.45; found: 821.564.

Synthesis of BN-PZ: BN-PZ was synthesized according to the same procedure as for BN-AC by using **M5** (1.00 g, 1.02 mmol) instead **M3**. BN-PZ (0.33 g, yield: 33.94%) was obtained as orange solid. ^{1}H NMR (400 MHz, CD$_2$Cl$_2$) δ 9.09 (s, 2H), 8.81 – 6.71 (m, 16H), 5.93 (d, J = 134.8 Hz, 6H), 1.60 (s, 18H), 1.43 (s, 18H), 1.34 (s, 9H). ^{13}C NMR (101 MHz, CD$_2$Cl$_2$) δ 145.89, 145.19, 141.55, 138.12, 129.87, 127.00, 124.66, 123.73, 121.09, 117.41, 114.26, 35.13, 34.69, 31.90, 31.49, 31.17, 29.68. MALDI-TOF-MS (m/z) of C$_{68}$H$_{69}$BN$_4$ for [M]$^+$, calcd: 952.56; found: 952.748.
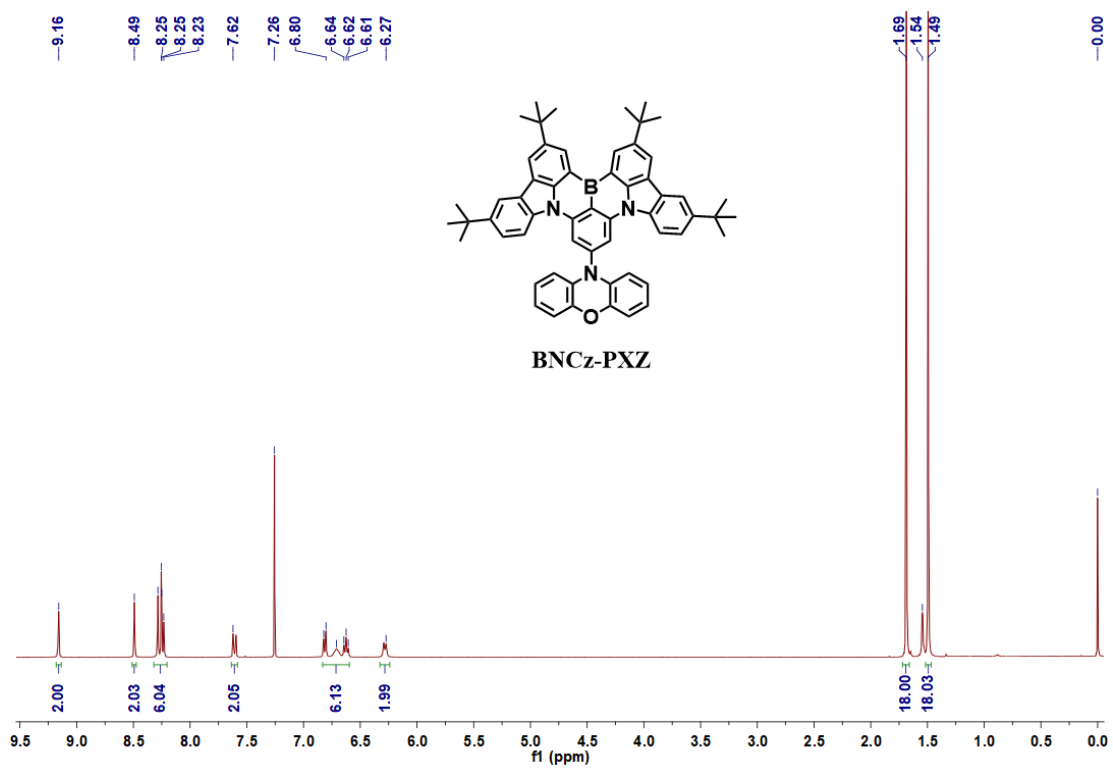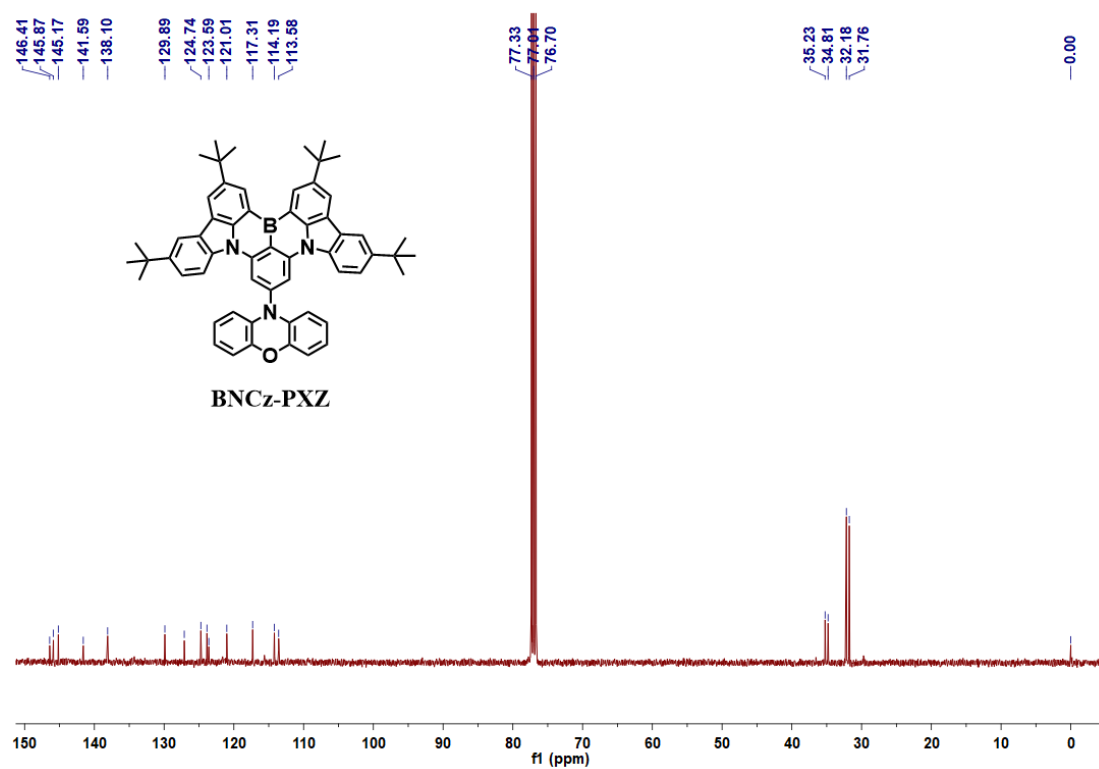
2. Supplementary Figures and Tables
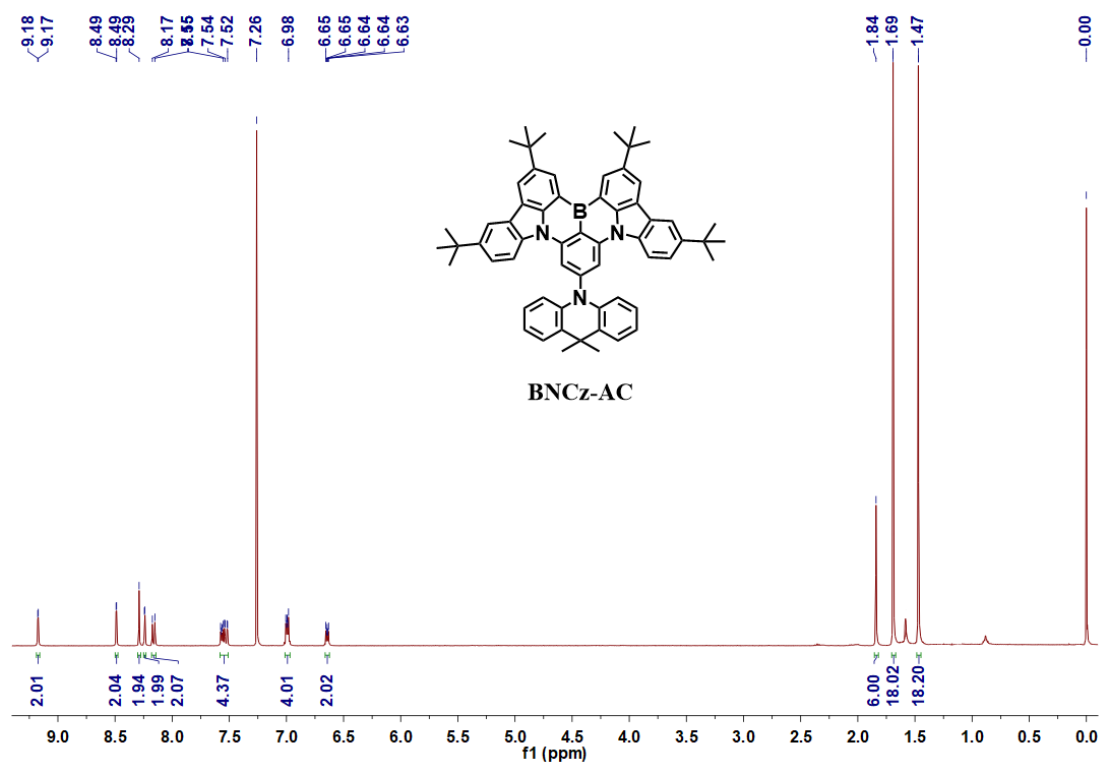
Figure S1. ^{1}H NMR spectrum of **BN-AC** measured in deuterated CDCl$_3$.
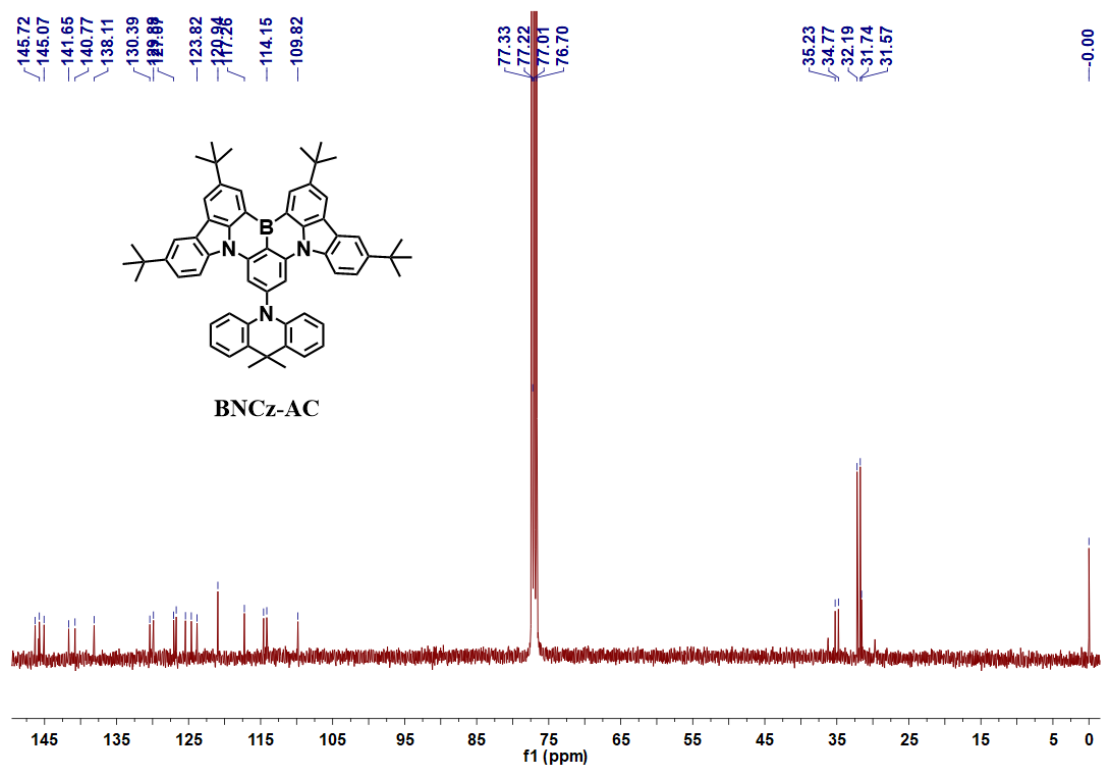
Figure S2. ^{13}C NMR spectrum of **BN-AC** measured in deuterated CDCl$_3$.

BNCz-PXZ

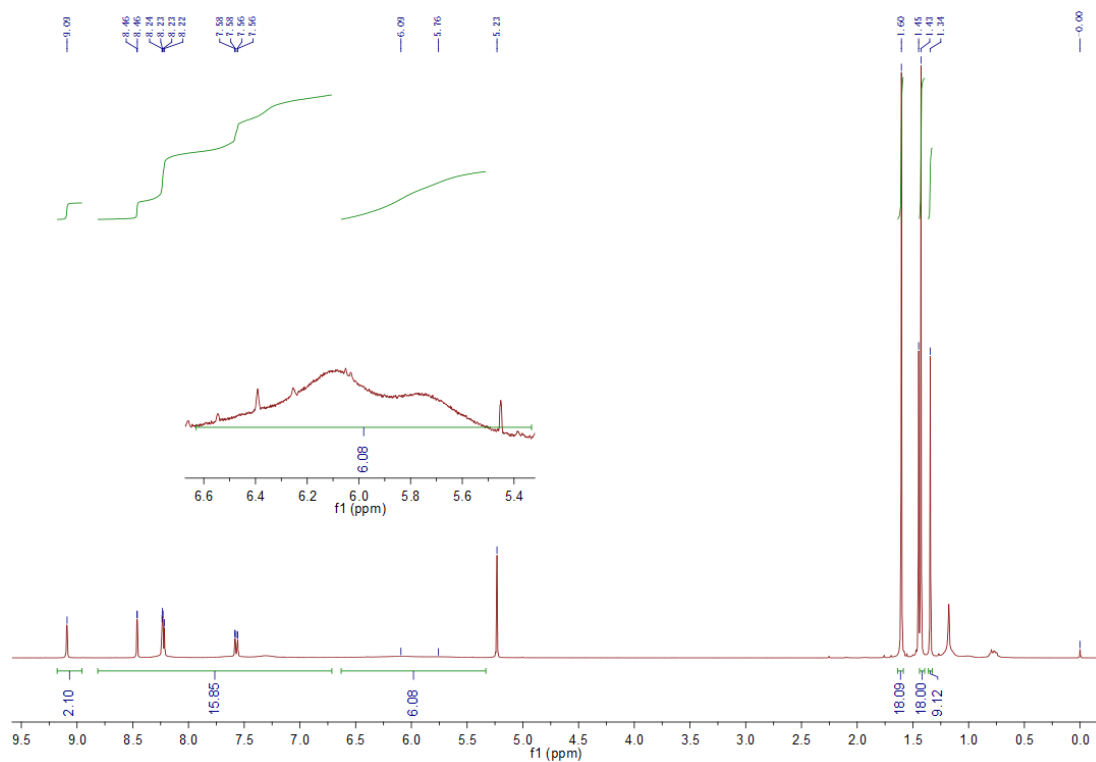**Figure S3.** ^{1}H NMR spectrum of **BN-PXZ** measured in deuterated CDCl$_3$.

Figure S4. ^{13}C NMR spectrum of **BN-PXZ** measured in deuterated CDCl$_3$.

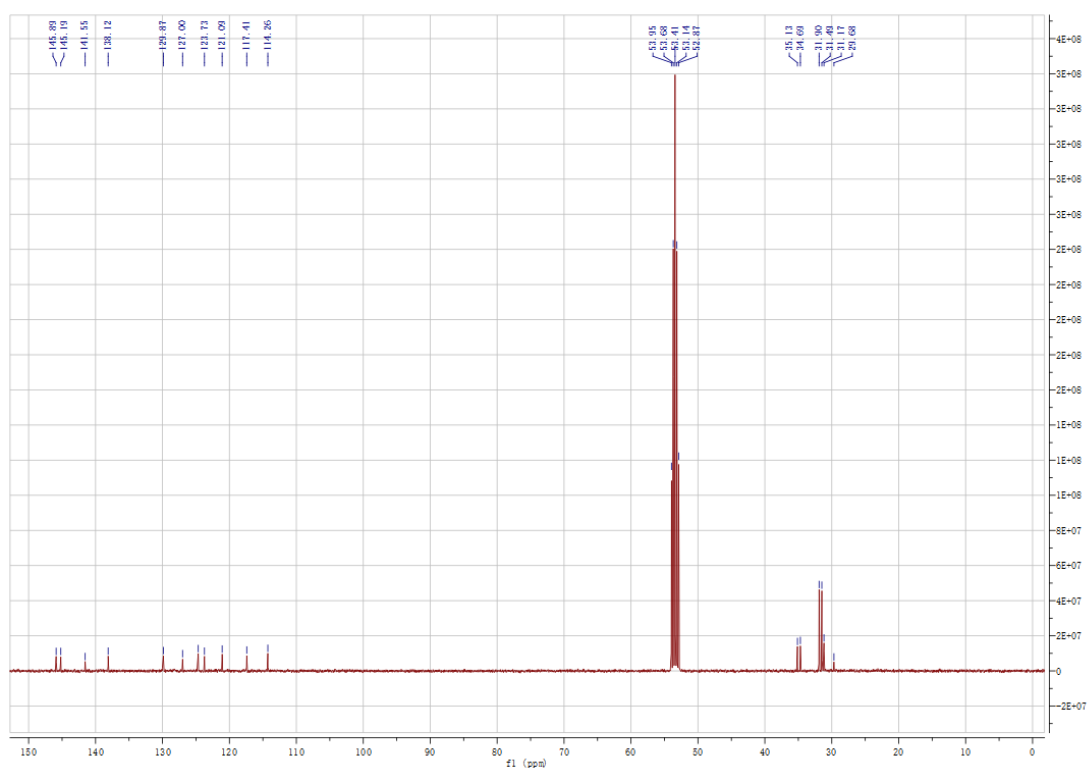**Figure S5.** ^{1}H NMR spectrum of **BN-PZ** measured in deuterated CD_2Cl_2.

Figure S6. ^{13}C NMR spectrum of **BN-PZ** measured in deuterated CD_2Cl_2.
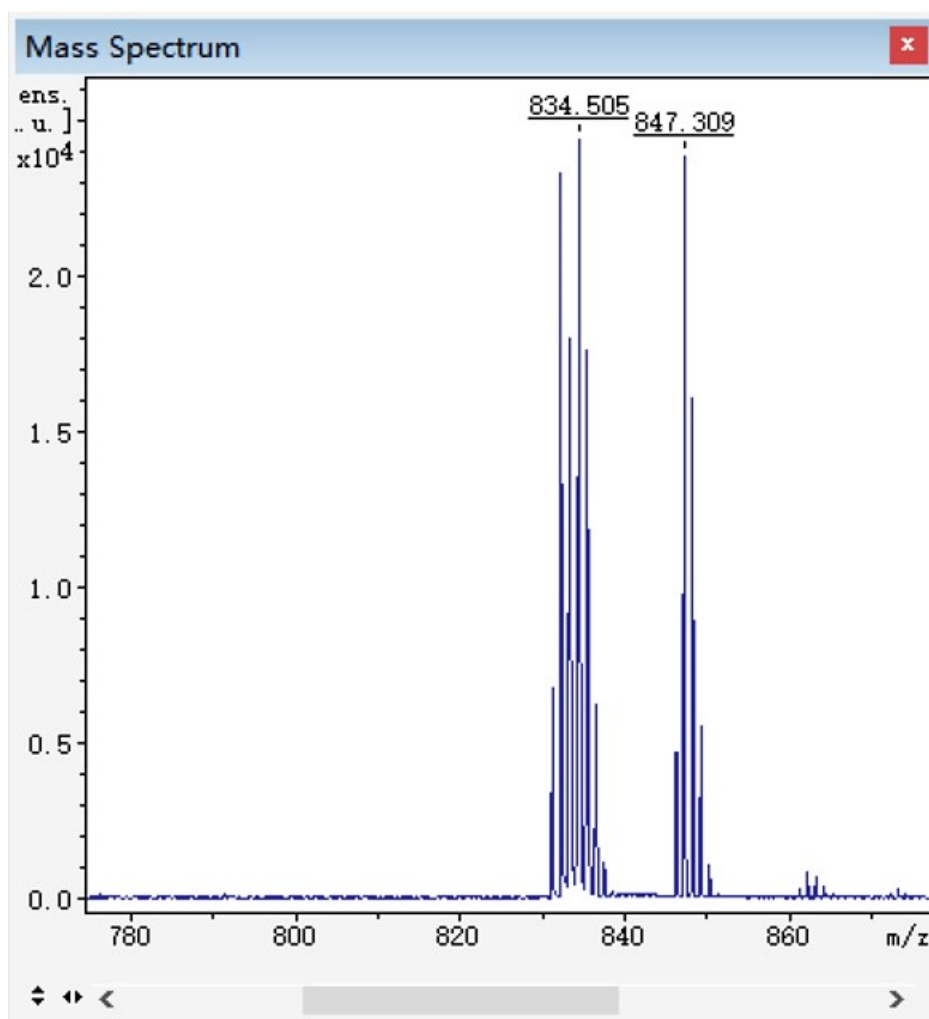
Figure S7. Mass spectrum of **BN-AC**.
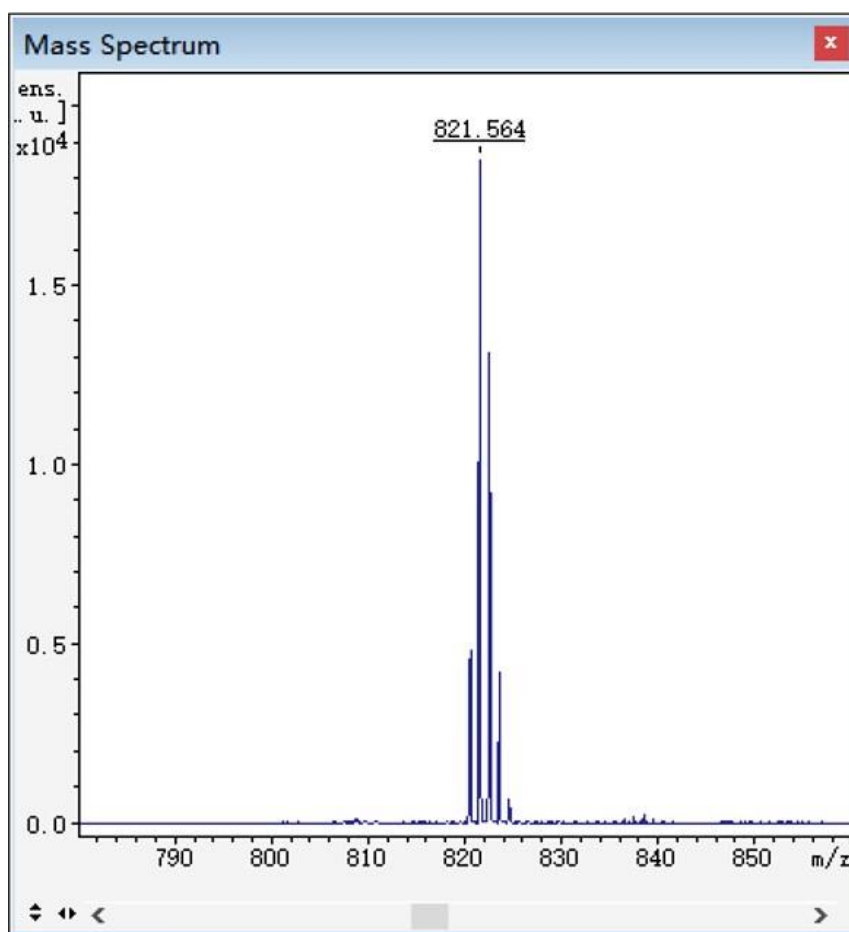
Figure S8. Mass spectrum of **BN-PXZ**.
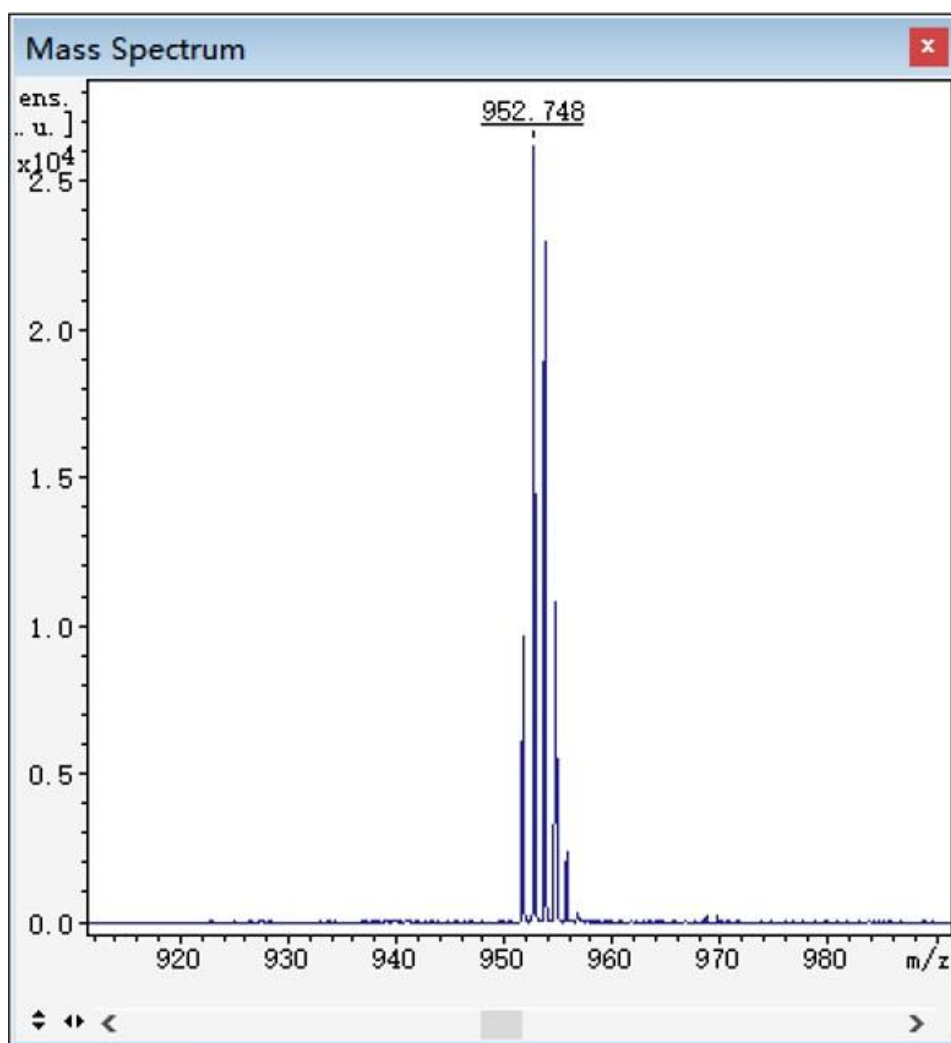
Figure S9. Mass spectrum of **BN-PZ**.
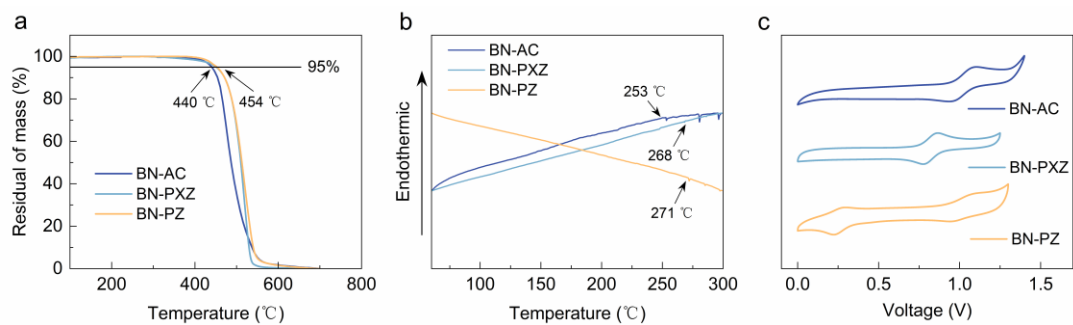
Figure S10. (a) TGA, (b) DSC traces and (c) cyclic voltammograms of **BN-AC**, **BN-PXZ** and **BN-PZ**.

Single-crystal structure   Dimer 1   Dimer 2
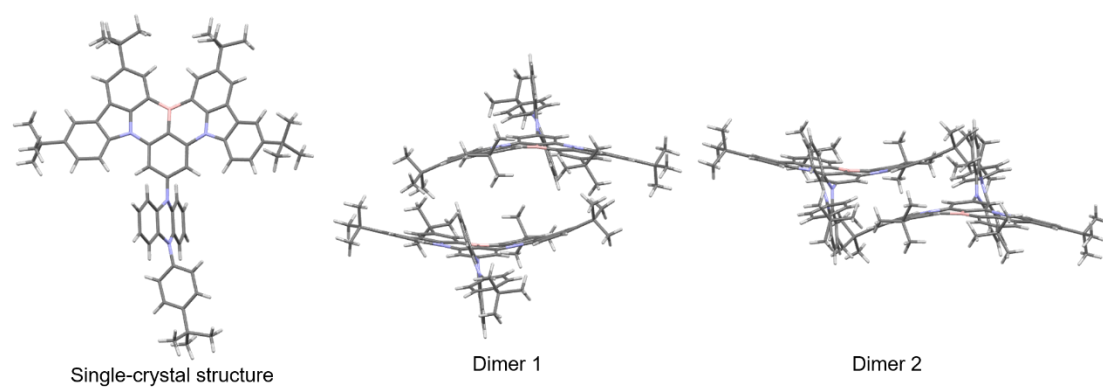
Figure S11. Single-crystal structure and dimer of **BN-PZ**.
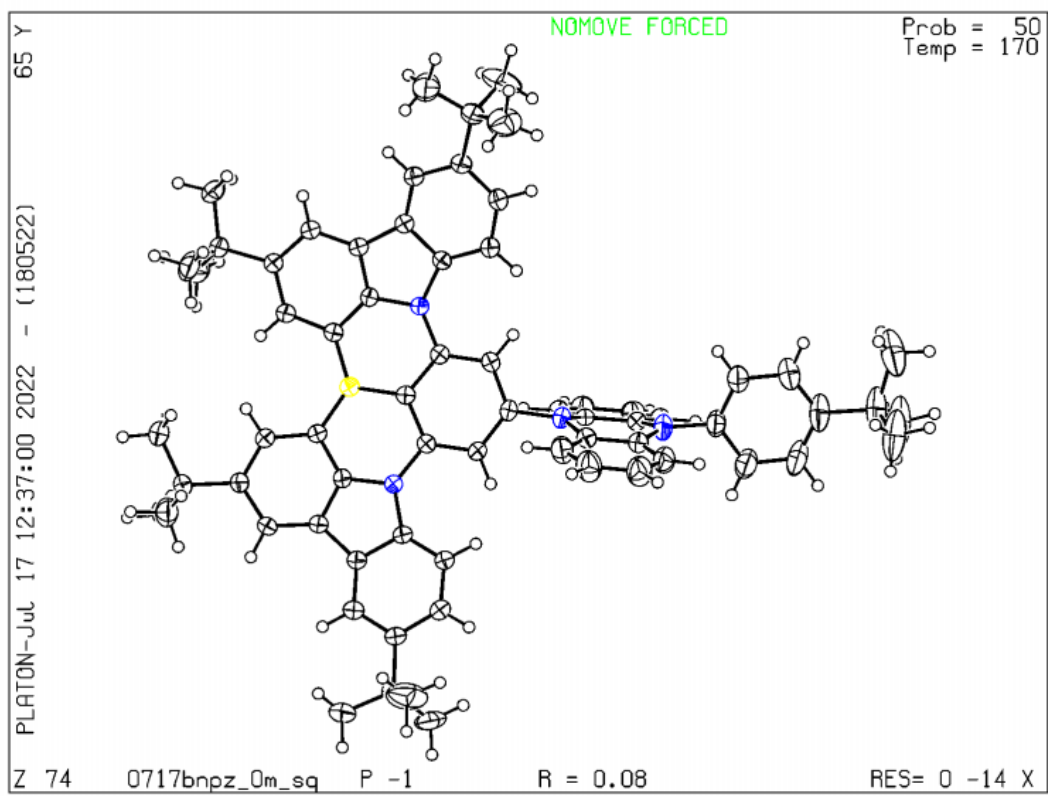
Figure S12. Single-crystal structure of **BN-PZ**.
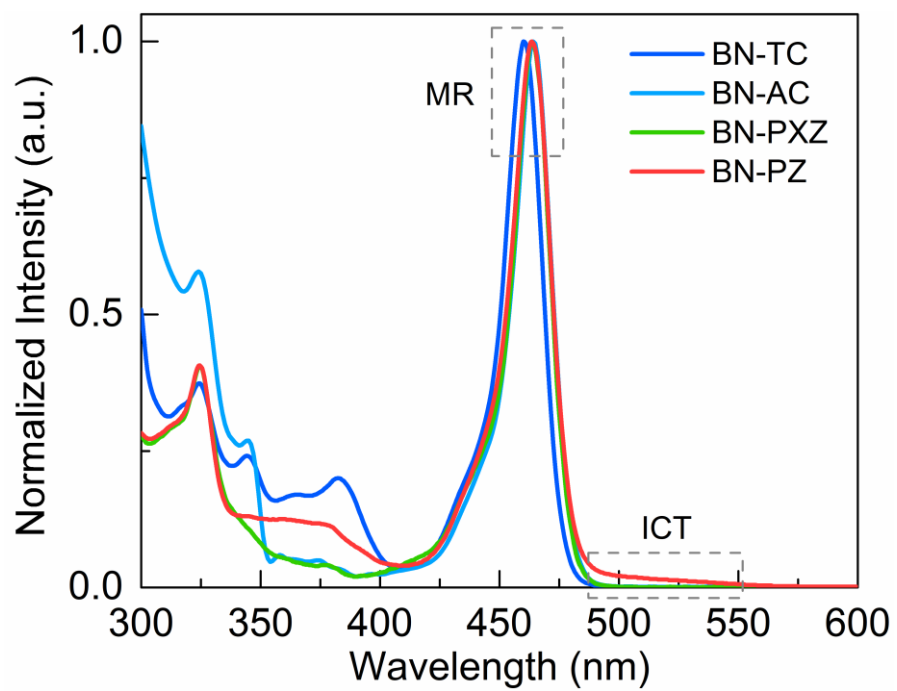
Figure S13. UV-vis absorption spectra of these emitters.
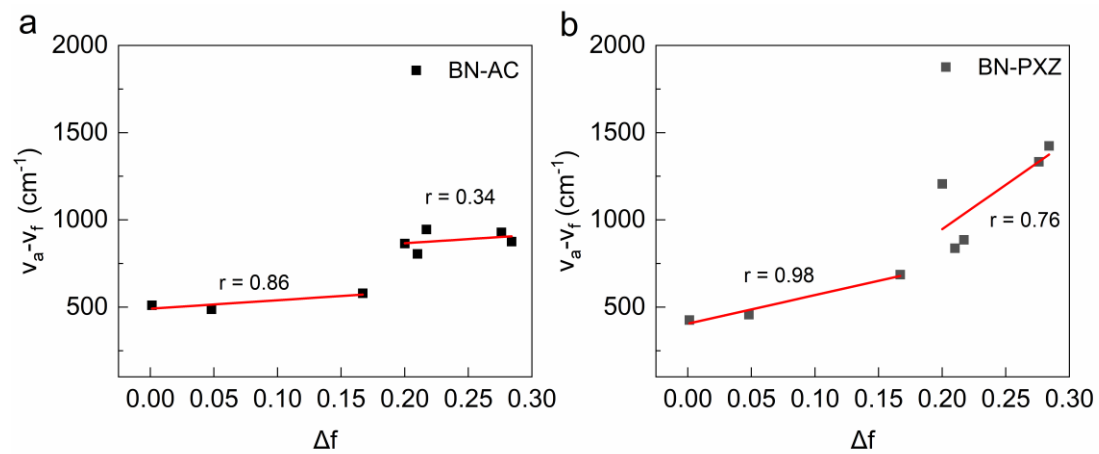
Figure S14. Solvatochromic Lippert-Mataga models of (a) **BN-AC** and (b) **BN-PXZ**.
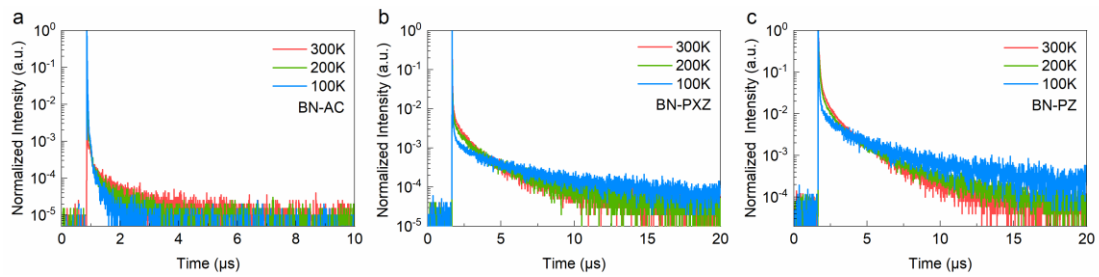
Figure S15. Temperature dependent time resolved photoluminescence spectra of BN-AC, BN-PXZ and BN-PZ.
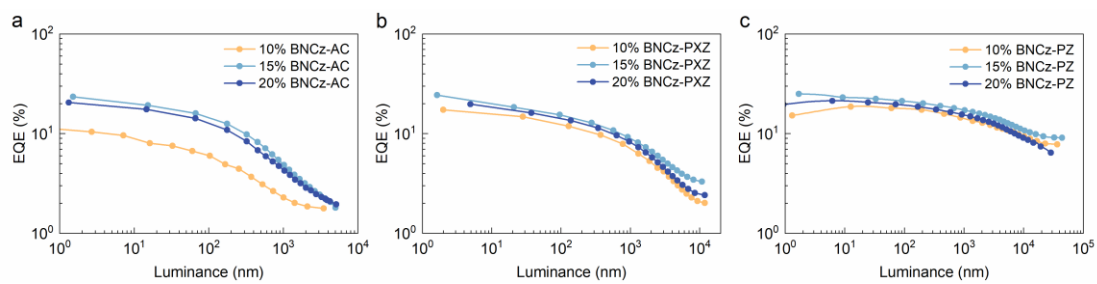
Figure S16. External quantum efficiency versus luminance (EQE-L) curves of the devices based on (a) BNCz-AC, (b) BNCz-PXZ and (c) BNCz-PZ with the doping concentration of 10, 15 and 20 wt%.
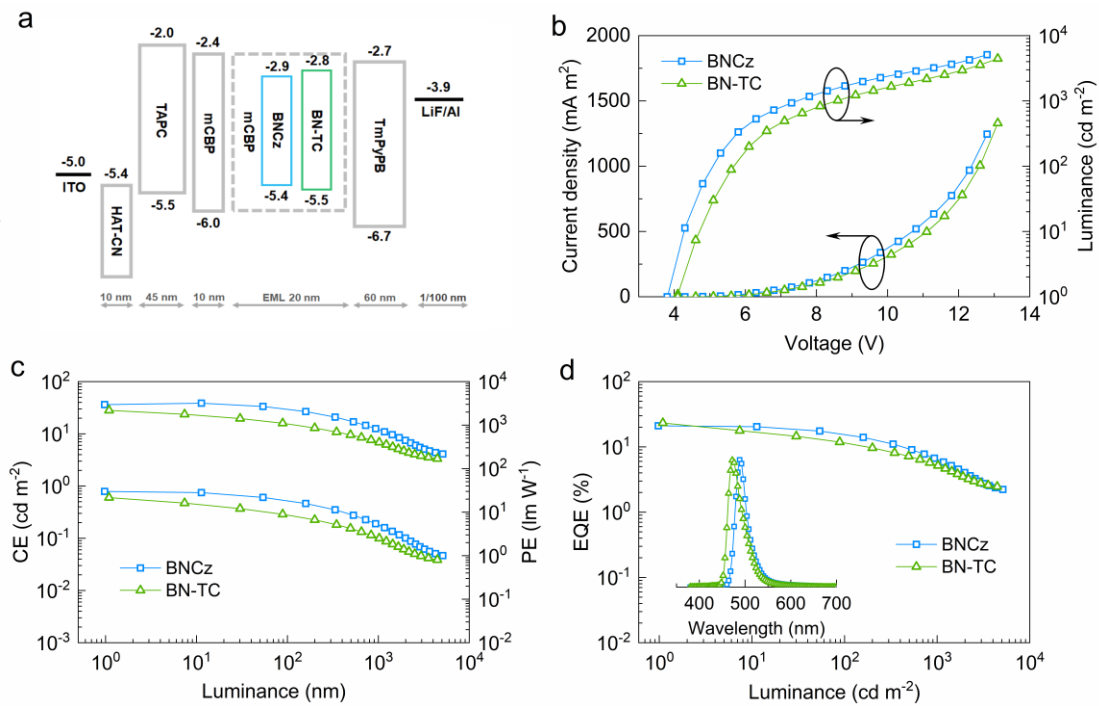
Figure S17. (a) Device structure and energy level diagram of the materials used. (b) Current density and luminance versus voltage (J-V-L). (c) Current efficiency and power efficiency versus luminance (CE-L-PE). (d) External quantum efficiency versus luminance (EQE-L) curves of the devices. (Inset: electroluminescence spectra of devices).
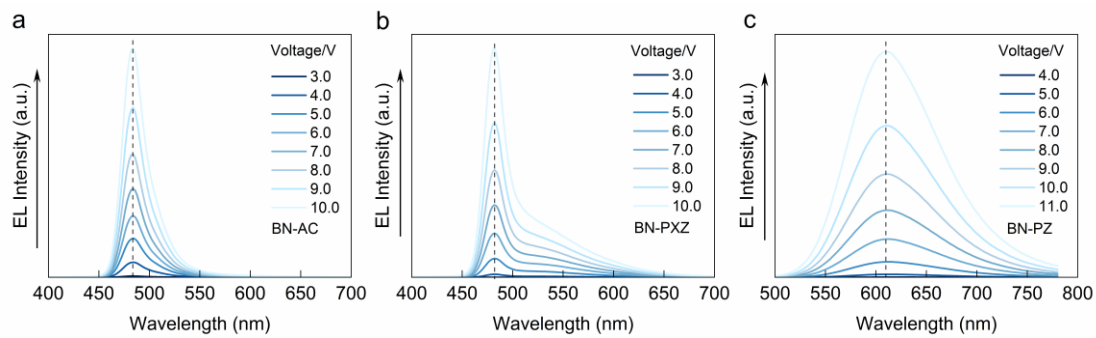
Figure S18. EL spectra of the devices based on (a) BN-AC, (b) BN-PXZ and (c) BN-PZ on different operating voltages.
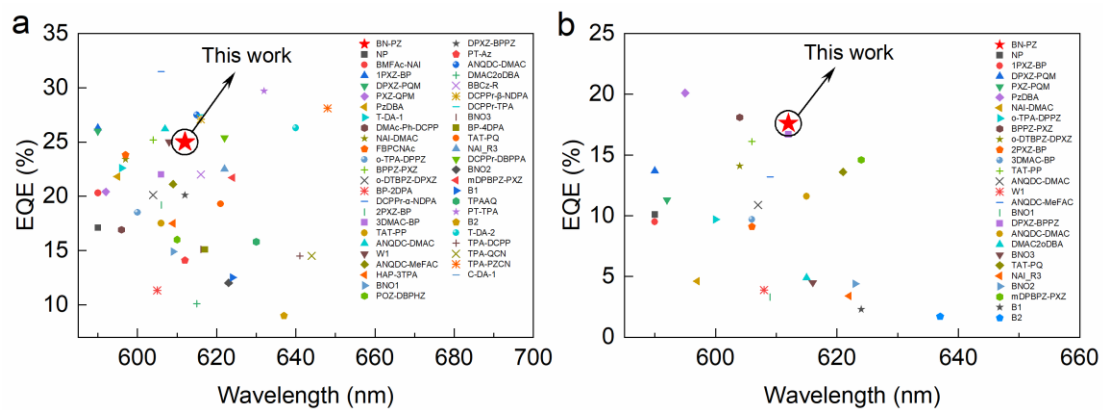
Figure S19. EQE summary of TADF-OLEDs with emission peaks from 590 nm to 650 nm without using TADF- or phosphor- sensitizing fluorescent technology. (a) Maximum EQE. (b) EQE at 1000 cd m^{-2}.

Table S1. Crystal data and structure refinement for **BN-PZ.**

Compound	BN-PZ
Empirical formula	C68H69BN4
Formula weight	953.08
Temperature/K	170.0
Crystal system	triclinic
Space group	P-1
a/Å	11.0353(5)
b/Å	13.6873(6)
c/Å	19.1898(8)
α/°	72.4450(10)
β/°	86.363(2)
γ/°	80.032(2)
Volume/Å^3	2721.6(2)
Z	2
ρcalcg/cm^3	1.163
μ/mm^{-1}	0.067
F(000)	1020.0
Crystal size/mm^3	$0.15 \times 0.08 \times 0.05$
Radiation	MoKα (λ = 0.71073)
2Θ range for data collection/°	4.336 to 52.812
Index ranges	$-13 \le h \le 13$, $-17 \le k \le 17$, $-23 \le l \le 21$
Reflections collected	31468
Independent reflections	11065 [R_{int} = 0.0887, R_{sigma} = 0.1185]
Data/restraints/parameters	11065/736/673
Goodness-of-fit on F^2	1.019
Final R indexes [I>=2σ (I)]	R_1 = 0.0799, wR_2 = 0.1762
Final R indexes [all data]	R_1 = 0.1705, wR_2 = 0.2283
Largest diff. peak/hole / e Å^{-3}	0.65/-0.28

Table S2. Solvatochromic UV-PL data for Lippert-Mataga model.

Solvents	Δf	BN-AC			BN-PXZ		
		ν_a	ν_f	ν_a-ν_f	ν_a	ν_f	ν_a-ν_f
Hexane	0.0012	460.5	471.6	511.12	460.0	469.2	426.26
Triethylamime	0.048	461.0	471.6	487.56	460.5	470.4	457.02
Ether	0.167	460.0	472.6	579.59	460.0	475.0	686.50
Ethyl acetate	0.2	460.5	479.6	864.82	460.5	487.6	1206.91
THF	0.21	462.5	480.4	805.63	462.0	480.6	837.70
Dichloromethane	0.217	463.0	484.2	945.65	463.0	482.8	885.76
DMF	0.276	463.0	483.8	928.57	464.0	494.6	1333.37
Acetone	0.284	461.0	480.4	875.99	461.0	493.4	1424.44
Acetonitrile	0.305	/	/	/	463.5	496.6	1438.04

Table S3. Summary of photophysical properties of **BN-AC**, **BN-PXZ** and **BN-PZ** in doped films.

Emitters	Φ_{PL} (%)[a]	Φ_p (%)[b]	Φ_d (%)[b]	τ_p (ns)[c]	τ_d (μs)[c]	k_r (10^7 s^{-1})[d]	k_{nr} (10^6 s^{-1})[d]	k_{ISC} (10^7 s^{-1})[d]	k_{RISC} (10^5 s^{-1})[d]
BN-AC	94	84	10	3.8	9.7	22.4	14.3	2.7	1.1
BN-PXZ	97	77	20	8.9	1.7	8.7	2.7	2.3	7.5
BN-PZ	98	45	53	39.4	1.2	1.2	0.24	1.3	18.5

[a] Total photoluminescence quantum yield (Φ_{PL}) with 15 wt % thin film doped in mCBP. [b] The contributions of the prompt component (Φ_P) and delayed (Φ_d) component. [c] The lifetime of prompt and delayed fluorescence. [d] The rate constants of radiative decay (k_r), non-radiative decay (k_{nr}), intersystem crossing (k_{ISC}) and reverse intersystem crossing (k_{RISC}).

Table S4. Performance summary of TADF-OLEDs with emission peaks from 590 nm to 650 nm without using TADF- or phosphor- sensitizing fluorescent technology.

Emitter	EL (nm)	V_{on} (V)	CE_{MAX} (cd A^{-1})	PE_{MAX} (lm W^{-1})	EQE_{max} (%)	EQE_{1000} (%)	Ref.
BN-PZ	**612**	**3.8**	**34.9**	**29.2**	**25.0**	**17.6**	**This**
NP	590	3.6	28.6	23.2	17.1	10.1	[S5]
BFMAc-NAI	590	3.0	49.2	51.4	20.3	--	[S6]
1PXZ-BP	590	2.6	47.2	57.1	26.3	9.5	[S7]
DPXZ-PQM	590	2.8	60.7	67.4	26.0	13.7	[S8]
PXZ-PQM	592	3.4	45.2	37.7	20.4	11.3	[S8]
PzDBA	595	2.7	35.7	--	21.8	20.1	[S9]
T-DA-1	596	3.0	51.2	53.6	22.6	--	[S10]
DMAc-Ph-	596	3.3	34.5	32.8	16.9	--	[S11]
NAI-DMAC	597	3.0	50.7	53.1	23.4	4.6	[S12]
FBPCNAc	597	--	55.7	57.8	23.8	--	[S13]
o-TPA-DPPZ	600	3.1	41.8	42.3	18.5	9.7	[S14]
BPPZ-PXZ	604	--	37.0	41.0	25.2	18.1	[S15]
o-DTBPZ-	604	3.5	38.1	29.2	20.1	14.1	[S16]
BP-2DPA	605	2.9	--	--	11.3	--	[S17]
DCPPr-α-	606	3.1	59.6	58.4	31.5	--	[S18]
2PXZ-BP	606	2.6	33.1	27.4	19.2	9.1	[S7]
3DMAC-BP	606	3.1	38.2	36.4	22.0	9.7	[S19]
TAT-PP	606	3.5	41.0	29.8	17.5	16.1	[S20]
ANQDC-	607	2.7	48.5	54.4	26.2	10.9	[S21]
W1	608	4.1	40.0	38.3	25.0	3.9	[S22]
ANQDC-	609	2.9	36.4	40.6	21.1	13.2	[S21]
HAP-3TPA	609	--	25.9	22.1	17.5	--	[S23]
BNO1	609	3.0	22.1	24.8	14.9	3.3	[S24]
POZ-DBPHZ	610	--	--	--	16.0	--	[S25]
DPXZ-BPPZ	612	3.1	30.2	30.9	20.1	16.7	[S26]
PT-Az	612		20.0	23.7	14.1	--	[S27]
ANQDC-	615	2.7	47.6	53.1	27.5	11.6	[S21]
DMAC2oDBA	615	3.4	13.8	14.4	10.1	4.9	[S28]
BBCz-R	616	--	--	--	22	--	[S29]

DCPPr-β-	616	3.1	42.4	41.6	27.1	--	[S18]
DCPPr-TPA	616	3.1	47.5	46.6	27.5	--	[S18]
BNO3	616	3.0	17.7	19.9	15.1	4.5	[S24]
BP-4DPA	617	2.7	--	--	15.1	--	[S17]
TAT-PQ	621	3.5	27.3	39.1	19.3	13.6	[S20]
NAI_R3	622	7.0	28.3	9.4	22.5	3.4	[S30]
DCPPr-DBPPA	622	3.3	40.1	37.0	25.4	--	[S18]
BNO2	623	3.0	12.8	16.8	12.0	4.4	[S24]
mDPBPZ-PXZ	624	--	25.0	21.0	21.7	14.6	[S15]
B1	624	--	--	--	12.5	2.3	[S31]
TPAAQ	630	--	--	--	15.8	--	[S32]
PT-TPA	632	--	30.0	38.5	29.7	--	[S27]
B2	637	--	--	--	9.0	1.7	[S31]
T-DA-2	640	3.0	24.4	22.5	26.3	--	[S10]
TPA-DCPP	641	2.9	15.6	15.3	14.5	--	[S33]
TPA-QCN	644	3.0	14.3	14.9	14.5	--	[S34]
TPA-PZCN	648	2.4	20.0	26.3	28.1	--	[S35]
C-DA-1	648	4.4	2.2	1.3	3.5	--	[S10]

3. References

S1.   D. H. Ahn, S. W. Kim, H. Lee, I. J. Ko, D. Karthik, J. Y. Lee and J. H. Kwon, Highly efficient blue thermally activated delayed fluorescence emitters based on symmetrical and rigid oxygen-bridged boron acceptors, Nat. Photonics, 2019, **13**, 540-546.

S2.   Q. Zhang, B. Li, S. Huang, H. Nomura, H. Tanaka and C. Adachi, Efficient blue organic light-emitting diodes employing thermally activated delayed fluorescence, *Nat. Photonics*, 2014, **8**, 326-332.

S3.   Y. Xu, C. Li, Z. Li, Q. Wang, X. Cai, J. Wei and Y. Wang, Constructing Charge-Transfer Excited States Based on Frontier Molecular Orbital Engineering: Narrowband Green Electroluminescence with High Color Purity and Efficiency, *Angew. Chem. Int. Ed.*, 2020, **59**, 17442-17446.

S4.   Y. Xu, Z. Cheng, Z. Li, B. Liang, J. Wang, J. Wei, Z. Zhang and Y. Wang, Molecular-Structure and Device-Configuration Optimizations toward Highly Efficient Green Electroluminescence with Narrowband Emission and High Color Purity, *Adv. Optical Mater.*, 2020, **8**, 1902142.

S5.   H. Liu, J. Li, W.-C. Chen, X. Lv, C. Zhou, C.-S. Lee and C. Yang, Efficient Yellow Thermally Activated Delayed Fluorescent Emitters Based on 3,5-Dicyanopyridine Acceptors, *J. Phys. Chem. C*, 2020, **124**, 25489-25498.

S6.   T. Chen, C.-H. Lu, C.-W. Huang, X. Zeng, J. Gao, Z. Chen, Y. Xiang, W. Zeng, Z. Huang, S. Gong, C.-C. Wu and C. Yang, Tuning the emissive characteristics of TADF emitters by fusing heterocycles with acridine as donors: highly efficient orange to red organic light-emitting diodes with EQE over 20%, *J. Mater. Chem. C*, 2019, **7**, 9087-9094.

S7.   F.-M. Xie, P. Wu, S.-J. Zou, Y.-Q. Li, T. Cheng, M. Xie, J.-X. Tang and X. Zhao, Efficient Orange–Red Delayed Fluorescence Organic Light-Emitting Diodes with External Quantum Efficiency over 26%, *Adv. Electron. Mater.*, 2020, **6**, 1900843.

S8.   J. Liang, C. Li, Y. Cui, Z. Li, J. Wang and Y. Wang, Rational design of efficient orange-red to red thermally activated delayed fluorescence emitters for OLEDs with external quantum efficiency of up to 26.0% and reduced efficiency roll-off, *J. Mater. Chem. C*, 2020, **8**, 1614-1622.

S9.   D. Karthik, Y. H. Jung, H. Lee, S. Hwang, B.-M. Seo, J.-Y. Kim, C. W. Han and J. H. Kwon, Acceptor–Donor–Acceptor-Type Orange–Red Thermally Activated Delayed Fluorescence Materials Realizing External Quantum Efficiency Over 30% with Low Efficiency Roll-Off, *Adv. Mater.*, 2021, **33**, 2007724.

S10.   T. Yang, Z. Cheng, Z. Li, J. Liang, Y. Xu, C. Li, Y. Wang, Improving the Efficiency of Red Thermally Activated Delayed Fluorescence Organic Light-Emitting Diode by Rational Isomer Engineering. *Adv. Funct. Mater.* 2020, **30**, 2002681.

S11.   S. Wang, Z. Cheng, X. Song, X. Yan, K. Ye, Y. Liu, G. Yang and Y. Wang, Highly Efficient Long-Wavelength Thermally Activated Delayed Fluorescence

OLEDs Based on Dicyanopyrazino Phenanthrene Derivatives, *ACS Appl. Mater. Interfaces*, 2017, **9**, 9892-9901.

S12. W. Zeng, H.-Y. Lai, W.-K. Lee, M. Jiao, Y.-J. Shiu, C. Zhong, S. Gong, T. Zhou, G. Xie, M. Sarma, K.-T. Wong, C.-C. Wu and C. Yang, Achieving Nearly 30% External Quantum Efficiency for Orange–Red Organic Light Emitting Diodes by Employing Thermally Activated Delayed Fluorescence Emitters Composed of 1,8-Naphthalimide-Acridine Hybrids, *Adv. Mater.*, 2018, **30**, 1704961.

S13. S. Kothavale, W. J. Chung and J. Y. Lee, Rational Molecular Design of Highly Efficient Yellow-Red Thermally Activated Delayed Fluorescent Emitters: A Combined Effect of Auxiliary Fluorine and Rigidified Acceptor Unit, *ACS Appl. Mater. Interfaces*, 2020, **12**, 18730-18738.

S14. H. Wang, B. Zhao, P. Ma, Z. Li, X. Wang, C. Zhao, X. Fan, L. Tao, C. Duan, J. Zhang, C. Han, G. Chen and H. Xu, A red thermally activated delayed fluorescence emitter employing dipyridophenazine with a gradient multi-inductive effect to improve radiation efficiency, *J. Mater. Chem. C*, 2019, **7**, 7525-7530.

S15. J.-X. Chen, W.-W. Tao, W.-C. Chen, Y.-F. Xiao, K. Wang, C. Cao, J. Yu, S. Li, F.-X. Geng, C. Adachi, C.-S. Lee and X.-H. Zhang, Red/Near-Infrared Thermally Activated Delayed Fluorescence OLEDs with Near 100 % Internal Quantum Efficiency, *Angew. Chem. Int. Ed.*, 2019, **58**, 14660-14665.

S16. J.-X. Chen, Y.-F. Xiao, K. Wang, D. Sun, X.-C. Fan, X. Zhang, M. Zhang, Y.-Z. Shi, J. Yu, F.-X. Geng, C.-S. Lee and X.-H. Zhang, Managing Locally Excited and Charge-Transfer Triplet States to Facilitate Up-Conversion in Red TADF Emitters That Are Available for Both Vacuum- and Solution-Processes, *Angew. Chem. Int. Ed.*, 2021, **60**, 2478-2484.

S17. K. R. Naveen, S. J. Hwang, H. Lee and J. H. Kwon, Narrow Band Red Emission Fluorophore with Reasonable Multiple Resonance Effect, *Adv. Electron. Mater.*, 2022, **8**, 2101114.

S18. Z. Cai, X. Wu, H. Liu, J. Guo, D. Yang, D. Ma, Z. Zhao and B. Z. Tang, Realizing Record-High Electroluminescence Efficiency of 31.5 % for Red Thermally Activated Delayed Fluorescence Molecules, *Angew. Chem. Int. Ed.*, 2021, **60**, 23635-23640.

S19. F.-M. Xie, H.-Z. Li, G.-L. Dai, Y.-Q. Li, T. Cheng, M. Xie, J.-X. Tang and X. Zhao, Rational Molecular Design of Dibenzo[a,c]phenazine-Based Thermally Activated Delayed Fluorescence Emitters for Orange-Red OLEDs with EQE up to 22.0%, *ACS Appl. Mater. Interfaces*, 2019, **11**, 26144-26151.

S20. J. Fan, J. Miao, N. Li, Y. Zeng, C. Ye, X. Yin and C. Yang, A dual rigid donor and acceptor enabling red thermally activated delayed fluorescence emitters for efficient OLEDs with low efficiency roll-off, *J. Mater. Chem. C*, 2022, **10**, 10255-10261.

S21. X. Gong, P. Li, Y.-H. Huang, C.-Y. Wang, C.-H. Lu, W.-K. Lee, C. Zhong, Z. Chen, W. Ning, C.-C. Wu, S. Gong and C. Yang, A Red Thermally Activated Delayed Fluorescence Emitter Simultaneously Having High

Photoluminescence Quantum Efficiency and Preferentially Horizontal Emitting Dipole Orientation, *Adv. Funct. Mater.*, 2020, **30**, 1908839.

S22. Y.-Y. Wang, Y.-L. Zhang, K. Tong, L. Ding, J. Fan and L.-S. Liao, Highly efficient red thermally activated delayed fluorescence materials based on a cyano-containing planar acceptor, *J. Mater. Chem. C*, 2019, **7**, 15301-15307.

S23. J. Li, T. Nakagawa, J. MacDonald, Q. Zhang, H. Nomura, H. Miyazaki and C. Adachi, Highly Efficient Organic Light-Emitting Diode Based on a Hidden Thermally Activated Delayed Fluorescence Channel in a Heptazine Derivative, *Adv. Mater.*, 2013, **25**, 3319-3323.

S24. Y. Zou, J. Hu, M. Yu, J. Miao, Z. Xie, Y. Qiu, X. Cao and C. Yang, High-Performance Narrowband Pure-Red OLEDs with External Quantum Efficiencies up to 36.1% and Ultralow Efficiency Roll-Off, *Adv. Mater.*, 2022, **34**, 2201442.

S25. P. Data, P. Pander, M. Okazaki, Y. Takeda, S. Minakata and A. P. Monkman, Dibenzo[a,j]phenazine-Cored Donor–Acceptor–Donor Compounds as Green-to-Red/NIR Thermally Activated Delayed Fluorescence Organic Light Emitters, *Angew. Chem. Int. Ed.*, 2016, **55**, 5739-5744.

S26. J.-X. Chen, K. Wang, C.-J. Zheng, M. Zhang, Y.-Z. Shi, S.-L. Tao, H. Lin, W. Liu, W.-W. Tao, X.-M. Ou and X.-H. Zhang, Red Organic Light-Emitting Diode with External Quantum Efficiency beyond 20% Based on a Novel Thermally Activated Delayed Fluorescence Emitter, *Adv. Sci.*, 2018, **5**, 1800436.

S27. Y.-Y. Wang, K.-N. Tong, K. Zhang, C.-H. Lu, X. Chen, J.-X. Liang, C.-K. Wang, C.-C. Wu, M.-K. Fung and J. Fan, Positive impact of chromophore flexibility on the efficiency of red thermally activated delayed fluorescence materials, *Mater. Horiz.*, 2021, **8**, 1297-1303.

S28. A. Kumar, H. Y. Shin, T. Lee, J. Jung, B. J. Jung and M. H. Lee, Doubly Boron-Doped TADF Emitters Decorated with ortho-Donor Groups for Highly Efficient Green to Red OLEDs, *Chem. Eur. J.*, 2020, **26**, 16793-16801.

S29. M. Yang, I. S. Park and T. Yasuda, Full-Color, Narrowband, and High-Efficiency Electroluminescence from Boron and Carbazole Embedded Polycyclic Heteroaromatics, *J. Am. Chem. Soc.*, 2020, **142**, 19468-19472.

S30. W. Zeng, T. Zhou, W. Ning, C. Zhong, J. He, S. Gong, G. Xie and C. Yang, Realizing 22.5% External Quantum Efficiency for Solution-Processed Thermally Activated Delayed-Fluorescence OLEDs with Red Emission at 622 nm via a Synergistic Strategy of Molecular Engineering and Host Selection, *Adv. Mater.*, 2019, **31**, 1901404.

S31. Q. Zhang, H. Kuwabara, W.-J. Potscavage, S. Huang, Y. Hatae, T. Shibata, C. Adachi, Anthraquinone-Based Intramolecular Charge-Transfer Compounds: Computational Molecular Design, Thermally Activated Delayed Fluorescence, and Highly Efficient Red Electroluminescence. *J. Am. Chem. Soc.* 2014, **136**, 18070-18081.

S32. J. Xue, Q. Liang, R. Wang, J. Hou, W. Li, Q. Peng, Z. Shuai and J. Qiao, Highly Efficient Thermally Activated Delayed Fluorescence via J-Aggregates

with Strong Intermolecular Charge Transfer, *Adv. Mater.*, 2019, **31**, 1808242.

S33.   Y. Sun, W. Sun, W. Liu, X. Li, J. Yin and L. Zhou, Efficient Nondoped Pure Red/Near-Infrared TADF OLEDs by Designing and Adjusting Double Quantum Wells Structure, *ACS Appl. Electron Mater.*, 2022, **4**, 3615-3622.

S34.   C. Li, R. Duan, B. Liang, G. Han, S. Wang, K. Ye, Y. Liu, Y. Yi and Y. Wang, Deep-Red to Near-Infrared Thermally Activated Delayed Fluorescence in Organic Solid Films and Electroluminescent Devices, *Angew. Chem. Int. Ed.*, 2017, **56**, 11525-11529.

S35.   Y.-L. Zhang, Q. Ran, Q. Wang, Y. Liu, C. Hänisch, S. Reineke, J. Fan and L.-S. Liao, High-Efficiency Red Organic Light-Emitting Diodes with External Quantum Efficiency Close to 30% Based on a Novel Thermally Activated Delayed Fluorescence Emitter, *Adv. Mater.*, 2019, **31**, 1902368.